# Chapter 3

# Spectroscopy of beryllium isotopes

## 3.1 Theoretical considerations for the Be-isotopes

### 3.1.1 Cluster model

It is well known that in the $N = Z$ region a well developed cluster structure appears for lithium and beryllium isotopes. Typical examples of this are the $\alpha$-$\alpha$ structure of $^{8}$Be and the $\alpha$-$t$ structure of $^{7}$Li [Ike80]. Many theoretical studies using the cluster model have been successfully made both for structure problems and for nuclear reaction problems. However, a small part of these theoretical investigations have calculated the structure of these nuclei without assuming the existence of clusters. Below, the method of antisymmetrised molecular dynamics is described briefly. This is a microscopic model which is free of any assumption about the existence of clustering and starts from the nucleon-nucleon interaction alone.

### 3.1.2 Antisymmetrised Molecular Dynamics

This theoretical method was developed by Akira Ono *et al.* for the study of nuclear reactions [Ono92a, Ono92b, Ono93b, Ono93a, Ono95]. With Kanada En'yo this work was extended and applied very successfully to the study of nuclear structures [KE95b, KE95a, Dot97, KE98a, KE99]. The method of Antisymmetrised Molecular Dynamics (AMD) has already proved to be a powerful theoretical tool for the study of the ground states as well as excited states in light nuclei.

#### The simplest version of AMD for the study of nuclear structure

The wave function of a system can be written as a linear combination of AMD wave functions:

$$\Phi = c\Phi_{AMD} + c^{'}\Phi^{'}_{AMD} + .... \tag{3.1}$$

where the wave function of a nucleus with mass number $A$ is a Slater determinant of Gaussian wave packets:

$$\Phi_{AMD}(Z) = \frac{1}{\sqrt{A!}}\mathcal{A}\left\{\varphi_1, \varphi_2, ..., \varphi_A\right\},$$

$$\varphi_i = \phi_{X_i}\mathcal{X}_{\xi_i}\tau_i : \begin{cases} \Phi_{X_i}(r_j) \propto exp\left[-\nu\left(r_j - \frac{X_i}{\sqrt{\nu}}\right)^2\right], \\ \mathcal{X}_i = \begin{pmatrix} \frac{1}{2} + \xi_1 \\ \frac{1}{2} - \xi_1 \end{pmatrix}, \end{cases}$$

where the $i$-th single-particle wave function $\varphi_i$ is a product of the spatial wave function $\phi_{Xi}$, the intrinsic spin function $\mathcal{X}_{\xi_i}$ and the isospin function $\tau_i$. In this version of AMD the isospin function is fixed to be up for protons and down for neutrons. Thus, an AMD wave function is parametrised by a set of complex parameters $Z \equiv \{X_{ni}, \xi_i\}(n = 1, 3 \text{ and } i = 1, A)$, where the $X_i$'s indicate the centres of Gaussians for the spatial part and the $\xi_i$'s are the parameters for the directions of the intrinsic spins.

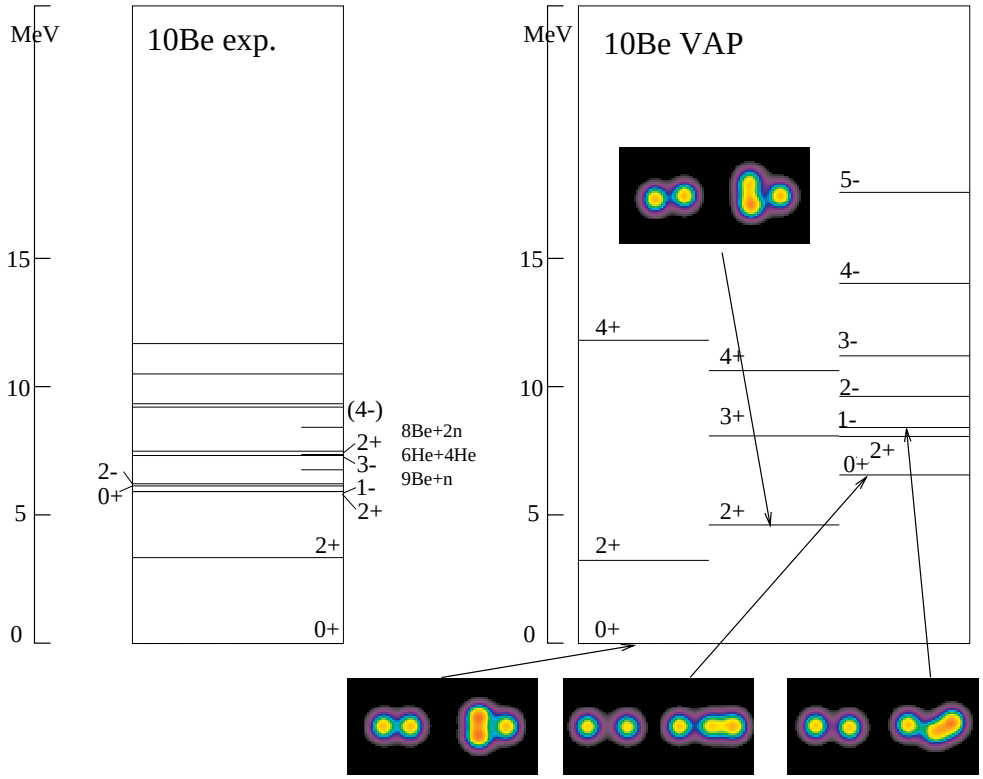


Figure 3.1: Excitation energies for the levels of $^{10}$Be [KE98b]. The theoretical results of the variational calculations after spin and parity projection (VAP) in the AMD (right) are compared with the experimental data (left) from Ref. [Rag89]. Density distributions of protons (neutrons) for the intrinsic states are also displayed in the left (right) columns of the black panels.

In the simplest version of AMD for the study of nuclear structure, the ground-state wave function of a system is obtained by the energy variation (using a cooling procedure to obtained the lowest state) of the parity projected eigenstate from a Slater determinant. Furthermore, the direction of intrinsic spins of single-particle wave functions are fixed to be up or down, $\xi_i = \pm\frac{1}{2}$, for simplicity. Therefore, the spin-isospin functions of the single-particle wave functions are chosen as p$\uparrow$, p$\downarrow$, n$\uparrow$ and n$\downarrow$ in the initial state and are fixed during the energy variation. In this case the total wave function of a system is parametrised only

by $X \equiv \{X_1, X_2, ..., X_A\}$, which are the centroids of Gaussian wave packets in the phase space. Finally, the state has to be projected to obtain states of good parity ($\pi$) and spin.

$$\Phi^{\pi}(X) = (1 \pm P)\Phi_{AMD}(X)$$

The minimum-energy state obtained with the energy variation for the parity projected state is considered as the intrinsic state of the system. After the intrinsic wave function is projected to obtain the total angular momentum, the expectation values of the electromagnetic operators and intrinsic density distributions of the nucleons can be obtained.

An example of these calculations is shown in Fig. 3.1. In the figure the excitation energy of the levels in $^{10}$Be are shown. The density distribution of protons is shown in the left part of the coloured panels and for the neutrons in the right part. As can be seen from the figure the protons and the neutrons are grouped into two parts which makes two $\alpha$-particles. Also, the neutron distribution for the levels is different with likely $\sigma$ and $\pi$ bond structure (see Fig. 3.2).

Higher excited states are constructed by superimposing two bases in order to orthogonise to the lower states. In this sense, in "the simplest version of AMD", as for the variational calculations after the parity projection, the full information on the excitation energy spectra is obtained.

### 3.1.3 Electromagnetic transition probabilities

When a nucleus emits $\gamma$ rays they are produced by the electromagnetic radiation field which can be described in terms of a multipole expansion [Bla59]. Here, only some basic aspects of multipole transitions which are used in this work are discussed. If the nucleus decays from a state with spin $I_i$ to a state with spin $I_f$, the total transition probability is given by:

$$T_{fi} = \frac{8\pi(L+1)}{\hbar L((2L+1)!!)^2}\left(\frac{E_\gamma}{\hbar c}\right)^{2L+1} B(\lambda L, I_i \rightarrow I_f) \qquad (3.2)$$

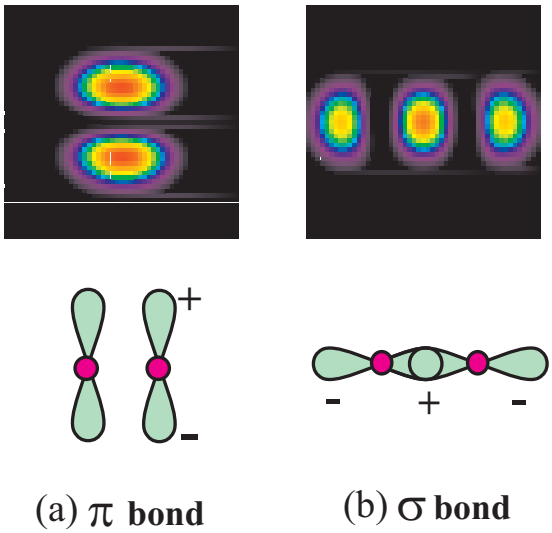


Figure 3.2: In the upper part of the picture, the density distributions of the valence neutron in the $0_1^+$ (top left) and $0_2^+$ (top right) states in $^{10}$Be [KE98b] are shown. The bottom part shows the corresponding schematic figures of the molecular orbits surrounding two clusters in the $\pi$ and $\sigma$ bonds respectively.

where the *reduced transition probabilities* $B(\lambda L)$ are given by

$$B(EL, I_i \to I_f) = \frac{1}{2I_i + 1} |\langle f \| \hat{Q} \| i \rangle|^2 \tag{3.3}$$

for the electric case and

$$B(ML, I_i \to I_f) = \frac{1}{2I_i + 1} |\langle f \| \hat{M} \| i \rangle|^2 \tag{3.4}$$

for the magnetic case. Here $\hat{Q}$ and $\hat{M}$ are the electric and magnetic multipole operators, respectively. It is assumed that the size of the radiation source (the nuclear radius) is much smaller that the wavelength of the emitted photon (the so called "long-wave approximation"). In order to take into account the different possible orientations of the angular momentum, $L$, an average over the initial and the final $m$-state values is taken. A detailed derivation of these equations can be found in [Rin80] and [Mor76].

The question of how many nucleons contribute to the radiation is very much related to the nuclear structure of the relevant states. There are two extreme

cases. The *single-particle* aspect, with the assumption that only one nucleon is excited and the *collective* aspect in which a large number of nucleons contribute coherently to the radiation.

### Weisskopf estimates

Beginning with the single-particle picture of the shell model where only one proton moves from one state to another, the transition probabilities $T(\lambda L)$ of multipolarity $L$ can be calculated in the case of electric transitions as:

$$T(EL) = \frac{8\pi(L+1)}{\hbar L((2L+1)!!)^2}\frac{e^2}{4\pi\epsilon_0\hbar c}\left(\frac{E_\gamma}{\hbar c}\right)^{2L+1}\left(\frac{3}{L+3}\right)^2 cR^{2L} \tag{3.5}$$

and for magnetic transitions:

$$T(ML) = \frac{8\pi(L+1)}{\hbar L((2L+1)!!)^2}\left(\mu_p - \frac{1}{L+1}\right)^2\left(\frac{\hbar}{m_p c}\right)^2\left(\frac{se^2}{4\pi\epsilon_0\hbar c}\right)\left(\frac{E_\gamma}{\hbar c}\right)^{2L+1}\left(\frac{3}{L+3}\right)^2 cR^{2L-2} \tag{3.6}$$

where $\mu_p$ is the magnetic moment of the proton, $m_p$ is the proton mass and the wave functions of the states are obtained using a square well potential. By setting the $\left(\mu_p - \frac{1}{L+1}\right)^2$ term to be equal to 10 and by taking $R = R_0 A^{1/3}$, estimates can be made for the lower multipole orders. These are known as the *Weisskopf single-particle estimates*, and are given in Table 3.1

| Weisskopf estimates | |
|---|---|
| $T^W(E1) = 1.02 \times 10^{14}\ A^{2/3}E^3$ | $T^W(M1) = 3.12 \times 10^{13}\ E^3$ |
| $T^W(E2) = 7.23 \times 10^{7}\ A^{4/3}E^5$ | $T^W(M2) = 2.21 \times 10^{7}\ A^{2/3}E^5$ |
| $T^W(E3) = 3.37 \times 10^{1}\ A^{2}E^7$ | $T^W(M3) = 1.03 \times 10^{1}\ A^{4/3}E^7$ |
| $T^W(E4) = 1.06 \times 10^{-5}\ A^{8/3}E^9$ | $T^W(M4) = 3.25 \times 10^{-6}\ A^{2}E^9$ |

Table 3.1: The Weisskopf estimates for the transition probabilities $T(\lambda L)$ in units of $s^{-1}$, where $\lambda$ is $E$ or $M$ and the energy values, $E$, are in MeV.

It is obvious that these estimates do not give a realistic calculation for the experimental transition rates, but they can be used as a scale. A transition is very often characterised by its transition probability in units of the Weisskopf estimate,

$$F_W = \frac{T\left(\lambda L\right)}{T^W\left(\lambda L\right)} = \frac{B\left(\lambda L\right)}{B^W\left(\lambda L\right)} \tag{3.7}$$

which is called the "*favoured factor*" or the "*enhancement factor*". Clearly, the Weisskopf estimate is very useful when an order of magnitude indication is of interest.

### Collective transition probabilities

The collective electric and magnetic transition rates for rotational nuclei were deduced by Bohr and Mottelson [Boh75]. Of interest for this work are mainly the $E1$ and $E2$ transitions. These are given by

$$B(E1, I_i \rightarrow I_f) = \frac{3}{4\pi} e^2 D_0^2 |\langle I_i K_i 10 | I_f K_f \rangle|^2, \tag{3.8}$$

and

$$B(E2, I_i \rightarrow I_f) = \frac{5}{16\pi} e^2 Q_0^2 |\langle I_i K_i 20 | I_f K_f \rangle|^2, \tag{3.9}$$

where $D_0$ and $Q_0$ are the intrinsic dipole and electric quadrupole moments, respectively and $K$ is the projection of the total angular momentum on the symmetry axis. The expressions in angled brackets are the Clebsch-Gordan coefficients.

In Table 3.2 the collective transition rate estimates given in terms of the reduced transition probabilities for the lowest multiplicities are shown. The estimates are obtained by multiplying out the constant terms in Equation 3.2. They are used in this work to obtain the transition probabilities for the observed and previously measured $\gamma$-ray transitions and for those for which only theoretically predicted $B(\lambda L)$ values are available. The results are given in Table 3.3.

| Collective transition probabilities | |
|---|---|
| $T(E1)= 1.59 \times 10^{15}\ E^3B(E1)$ | $T(M1)= 1.76 \times 10^{13}\ E^3B(M1)$ |
| $T(E2)= 1.22 \times 10^{9}\ E^5B(E2)$ | $T(M2)= 1.35 \times 10^{7}\ E^5B(M2)$ |
| $T(E3)= 5.67 \times 10^{2}\ E^7B(E3)$ | $T(M3)= 6.28 \times 10^{0}\ E^7B(M3)$ |
| $T(E4)= 1.69 \times 10^{-4}\ E^9B(E4)$ | $T(M4)= 1.87 \times 10^{-6}\ E^9B(M4)$ |

Table 3.2: Relation between the transition probability $T(\lambda L)$ and the reduced transition probability $B(\lambda L)$. Here $T(\lambda L)$ are in units of $s^{-1}$, $B(EL)$'s in $e^2fm^{2i}$ and $B(ML)$ in $\mu_N^2 fm^{2i-2}$.

The ratio between the electric dipole and the electric quadrupole moment can be extracted from the experimental data using the ratio of the reduced transition probabilities $B(E1)/B(E2)$. If the intensities of the $E1$ and $E2$ transitions are $i_{E1}$ and $i_{E2}$, respectively, then the $B(E1)/B(E2)$ ratio can be calculated using

$$\frac{i_{E1}}{i_{E2}} = \frac{1.59 \times 10^{15} E^3_{\gamma(E1)} B(E1)}{1.22 \times 10^{9} E^5_{\gamma(E2)} B(E2)}. \tag{3.10}$$

The ratio of the intrinsic dipole to the intrinsic quadrupole moment, $[D_0/Q_0]$, can be extracted using Equations (3.8) and (3.9) and the obtained $B(E1)/B(E2)$ ratio has the following form

$$\frac{B(E1)}{B(E2)} = 2.4 \left[ \frac{D_0}{Q_0} \frac{\langle I_i K_i 10 | I_f K_f \rangle}{\langle I_i K_i 20 | I_f K_f \rangle} \right]^2 \tag{3.11}$$

## 3.2 Search for $\gamma$-ray decays

For the isotopes of beryllium ($^{10-12}$Be) detailed $\gamma$-ray spectroscopic studies have not been reported before. With the advent of the new highly efficient $\gamma$-ray detector arrays a new search has been started. The nuclei are deformed in their ground states [vO97, KE95b] and it is expected that with the adding of further 'valence' neutrons to these deformed states a variety of new strongly deformed

| | $\mathbf{E}_\gamma$[MeV] | $\mathbf{B}(\lambda_i)$ | $\tau_\gamma$ | $\mathbf{J}\pi_i$ | $\mathbf{J}\pi_f$ | $\Gamma_\gamma\ [eV]$ | $\Gamma_{tot}\ [eV]$ | $\Gamma_\gamma/\Gamma_{tot}$ | $\lambda_i$ |
|---|---|---|---|---|---|---|---|---|---|
| $^{10}$**Be** | 3.367 | $(10.5^{+}_{-}1.2)$ | $(180^{+}_{-}17)$fs | $2^+_1$ | $0^+_1$(g.s) | $(3.66^{+}_{-}0.73).10^{-3}$ | | 1 | E2 |
| | 2.811 | $(3.3^{+}_{-}2)$ | $(1.1\text{ps}^{+0.4}_{-0.3})$ | $0^+_2$ | $2^+_1$ | $(4.6^{+}_{-}2.8).10^{-4}$ | $6.10^{-4}$ | 0.77 | E2 |
| | 0.219 | $(1.3^{+}_{-}0.6).10^{-2}$ | 4.6ps | $0^+_2$(g.s) | $1^-_1$ | $(1.4^{+}_{-}0.5).10^{-4}$ | $6.10^{-4}$ | 0.23 | E1 |
| | 1.363∗ | 35.72 | 4.88ps | $2^+_3$ | $0^+_2$ | $1.4.10^{-4}$ | $6.3.10^{3}$ | $2.1.10^{-8}$ | E2 |
| | 1.413∗ | 11.20 | 12.9ps | $3^-_1$ | $1^-_1$ | $5.1.10^{-5}$ | $15.7.10^{3}$ | $3.10^{-9}$ | E2 |
| $^{11}$**Be** | 1.29∗ | NN | NN | $5/2^-_2$ | $3/2^-_3$ | NN | NN | | E2;M1 |
| | 3.64∗ | 3.64 | 16ps | $3/2^-_1$ | $1/2^-_1$ | $4.2.10^{-3}$ | $15.10^{3}$ | $2.8.10^{-7}$ | E2 |
| | 4.93∗ | 8.06 | 34fs | $5/2^-_2$ | $1/2^-_1$ | $1.9.10^{-2}$ | $45.10^{3}$ | $4.2.10^{-7}$ | E2 |
| $^{12}$**Be** | 2.10∗ | 14.0 | 1.43ps | $2^+_1$ | $0^+_1$(g.s) | $4.6.10^{-4}$ | NN | | E2 |
| | 0.90∗ | 7.0 | 198ps | $2^+_3$ | $0^+_2$(g.s) | $4.6.10^{-4}$ | NN | | E2 |
| | 0.90∗ | 23.4 | 69ps | $2^+_3$ | $0^+_2$(g.s) | $1.1.10^{-5}$ | NN | | E2 |

Table 3.3: Branching ratios ($\Gamma_\gamma/\Gamma_{tot}$) for $\gamma$-ray decays in $^{10,11,12}$Be. The values are calculated using the formulae for the transition probabilities (see Section 3.1.3) and $\Gamma = \hbar/\tau$, where $\Gamma_\gamma$ and $\Gamma_{tot}$ are the $\gamma$-ray and total widths of the levels respectively and $\tau$ is the mean lifetime. Here, J$\pi_i$ is the spin and parity of the initial state and J$\pi_f$ is the spin and parity of the final state for a transition with multipolarity, $\lambda L$. Energies marked with '$*$' correspond to theoretical $B(\lambda L)$ values. A detailed discussion of the transitions is given in Section 3.2.

states can be formed. Recent discussions of the structure of some light neutron-rich nuclei have focused attention on the fact that strong clustering occurs close to the single-particle and cluster emission thresholds. The most likely structure of the strongly deformed shapes is related to the $\alpha$ clustering. Possible weak $\gamma$-ray decay branches are also expected in states above the particle thresholds. Measuring the $\gamma$-ray branches from these states will give a direct measure of their deformation.

Of particular interest is the search for $\gamma$-ray decay branches related to the dimer structure created by two $\alpha$ particles. Possible new $\gamma$-ray transitions as well as the rotational bands in the beryllium isotopes are shown in Fig. 3.3 and discussed below.

The electromagnetic transition probabilities between low-lying states and the ground state in $^{9}$Be have been measured only by electron inelastic scattering. Decay widths indicate that some of the corresponding $\gamma$-ray branches are within reach of the new Ge-detector-array facilities; for example the $5/2^-_1$ (2.43 MeV)$\rightarrow$ $3/2^-_1$(g.s.) transition has $\Gamma_\gamma = (8.9 \pm 1.0) \times 10^{-2}$eV which gives a branching ratio of $\Gamma_\gamma/\Gamma_{tot} \sim 10^{-4}$.

### 3.2.1 Expected transitions in $^{10}$Be

Even though the $\gamma$-spectroscopy of $^{10}$Be was made 30 years ago [Rou69], there is still great interest in weak $\gamma$-decay branches from states above the particle threshold, that could be measured. Some of them are given below.

**$E_\gamma$=1.108 MeV (M1),** $3^-_1$ *(7.37 MeV)*$\rightarrow$ $2^-_1$ *(6.236 MeV)*

This transition should have a large $B(M1)$ value, since both the initial and final states belong to the same rotational band, though none of the theoretical models of $^{10}$Be can predict the exact number. The $2^-_1 \rightarrow 1^-_1$ transition between the lowest members of the same band was studied decades ago [Rou69], but the result is not

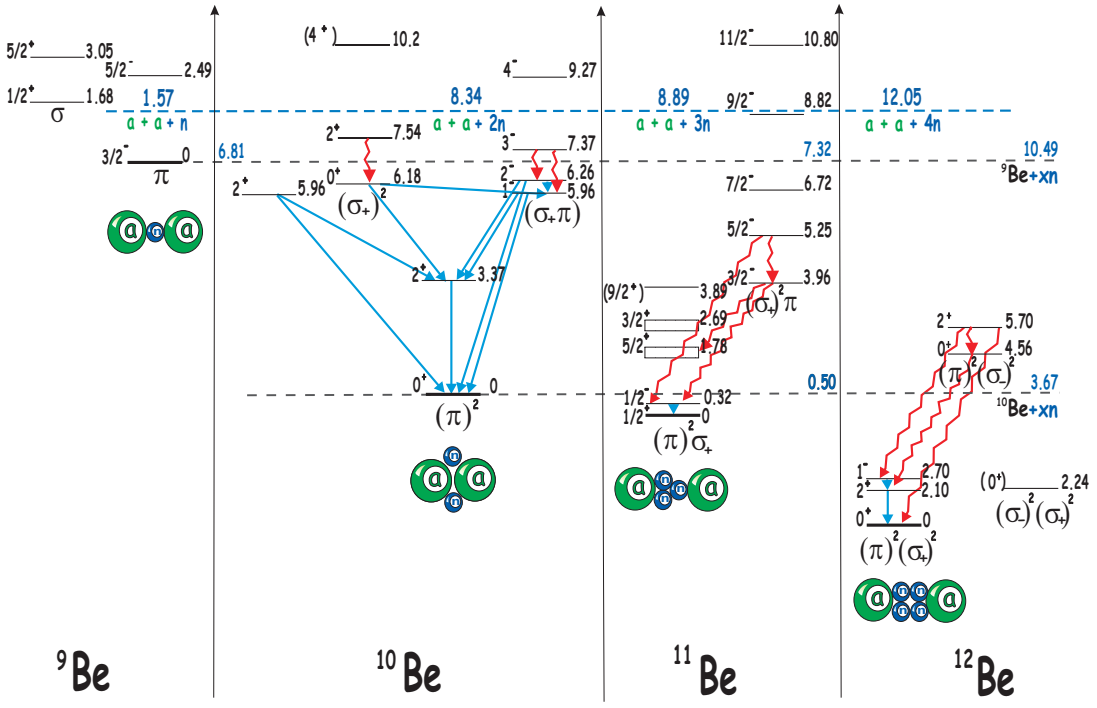


Figure 3.3: Plot of the excitation energies of known states in $^{9-12}$Be grouped into rotational bands where observed $\gamma$-ray transitions are shown with blue lines. This compilation is made in order to show the relation of the isomeric (molecular) shapes, expected close to the particle threshold. Possible new $\gamma$ decays are indicated by red lines.

clear and in fact only an upper limit for the branching ratio was set.

**$E_\gamma$=1.363 MeV (E2),** $2_3^+$*(7.542 MeV)*$\rightarrow$ $0_2^+$*(6.179 MeV)*

The $0_2^+$ state in $^{10}$Be is long-lived ($\tau_m$=1.1 ps) and it is assumed to be the bandhead of a molecular dimer band. It lives unusually long compared to the other lower lying states (with a typical lifetime of the order of femtoseconds), because of its shape, and $\gamma$-ray decays from the levels of this band with energies above the particle threshold will be very fast and compete with a retarded particle decay. The $2_3^+$ state is very narrow ($\Gamma$=6 keV) situated 700 keV above the threshold for neutron emission. It is assumed to have a deformed structure and there are some

hints that it decays through the $\alpha$+$^6$He channel. The neutron decay of this state is retarded due to the particular shape of the band relative to the ground state of $^9$Be. Itagaki and Okabe [Ita00] predict a huge $B(E2)$ value of 35.72 $e^2fm^4$ for this transition, in contrast to the transition to the ground state which is predicted to have $B(E2)$=0.19 $e^2fm^4$. AMD calculations [KE99] also predict a large $B(E2)$ value for this transition.

**E$_\gamma$=1.413 MeV (E2),** $3^-_1$ *(7.371 MeV)*$\rightarrow$ $1^-_1$ *(5.958 MeV)*

Kanada-En'yo *et al.* [KE95b] predict a rather large transition rate for this $\gamma$-ray branch, $B(E2)$=11.2 $e^2fm^4$, which reflects the fact that both the initial and final states are members of the same deformed rotational band.

### 3.2.2 Expected transitions in $^{11}$Be

A similar situation as that discussed for $^{10}$Be is expected. Possible $\gamma$-ray transitions are shown in Fig. 3.3 and discussed below :

**E$_\gamma$=1.29 MeV (E2),** $5/2^-_2$ *(5.25 MeV)*$\rightarrow$ $3/2^-_3$ *(3.96 MeV)*

These states are the first two states of the K=3/2 band which should be well deformed so that very large E2 transition rates (as for $^{10}$Be) can be expected.

**E$_\gamma$=3.64 MeV (E2),** $3/2^-_3$ *(3.96 MeV)*$\rightarrow$ $1/2^-_1$ *(0.32 MeV)*

The total width of the 3.96 MeV state is so small that it is not observable in charged particle spectroscopy [Boh99]. Since the AMD-calculations [KE95b] predict that the $B(E2)$ value for this transition should be relatively large (8.13 $e^2fm^4$), it is likely that the branching ratio for $\gamma$-ray emission could be large enough to detect.

**$E_\gamma$=4.93 MeV (E2),** $5/2_2^-$ *(5.25 MeV)*$\rightarrow$ $1/2_1^-$ *(0.32 MeV)*

The first excited state of the K=3/2 band at 3.96 MeV should have a larger particle-decay width than the second excited state (at 5.25 MeV), but the competing $\gamma$-decay may still be detectable, as the predicted $B(E2)$ value (8.06 $e^2fm^4$ [KE95b]) is relatively large.

### 3.2.3 Expected transitions in $^{12}$Be

Similar molecular states to those discussed for $^{10}$Be and $^{11}$Be with large deformations are predicted [KE95b] for $^{12}$Be. These states should have a $\gamma$-ray branch to the ground state or to the first excited $2^+$ state.

**$E_\gamma$=2.10 MeV (E2),** $2_1^+$ *(2.10 MeV)*$\rightarrow$ $0_1^+$ *(g.s.)*

Kanada En'yo *et al.* [KE95b] predict $B(E2)$= 14 $e^2fm^4$ for this transition. They also calculate a large number of new molecular states predicted at low excitation energies. These states should have a large probability to decay through $\gamma$-emission. Descouvemont and Baye [Des01] calculate a transition rate of just 6.6 Wu using microscopic $\alpha$+$^8$He and $^6$He + $^6$He wave functions for these levels, but they also predict two rotational bands based on $0_2^+$ and $1_1^-$ states with large probabilities for intraband transitions. For example, the $3_1^- \rightarrow 1_1^-$ transition has a predicted value of $B(E2)$=31.1 Wu.

**$E_\gamma$=0.90 MeV (E2),** $2_3^+$ *(7.3 MeV)*$\rightarrow$ $0_2^+$ *(6.4 MeV)*

For the second $K^\pi=0_1^+$ band, which consists of the closed p-shell states, Kanada En'yo *et al.* [KE95b] predict a small $B(E2)$ value of 7 $e^2fm^4$, while Descouvemont and Baye [Des01] predict 23.4 $e^2fm^4$.

The experiment described below was made to search for the weak $\gamma$-decay properties of these beryllium nuclei.

## 3.3 The $^{7}$Li + $^{10}$Be experiment

The population of strongly deformed structures in direct reactions is possible if the projectile and/or target already exhibit strong clustering. Accordingly, a neutron-rich $^{10}$Be target and a beam of $^{7}$Li have been chosen. A thick target experiment has been performed at the Laboratori Nazionali di Legnaro (LNL) in Italy, bombarding a $^{10}$BeO target with a $^{7}$Li beam. Gamma-ray events were collected using GASP in conjunction with the ISIS charged particle detector (for details see Chapter 2). This enabled channel selection by the observation of $\gamma$-$\gamma$-particle coincidences. For example the following reactions can be observed:

$$
\begin{aligned}
(^{7}\mathrm{Li}+^{10}\mathrm{Be})\rightarrow \quad & (^{4}\mathrm{He}+\mathrm{p})+^{12}\mathrm{Be} \\
& (^{4}\mathrm{He}+\mathrm{np})+^{11}\mathrm{Be} \\
& (^{4}\mathrm{He}+2\mathrm{np})+^{10}\mathrm{Be} \\
& (^{4}\mathrm{He})+^{13}\mathrm{B} \\
& (^{3}\mathrm{He};\ \mathrm{d}+\mathrm{p})+^{14}\mathrm{B} \\
& (2\mathrm{p})+^{15}\mathrm{B} \\
& (\mathrm{p})+^{16}\mathrm{C}
\end{aligned}
$$

The total thickness of the Be-Oxide target [Goo74b], which has an enrichment of >94% in $^{10}$Be, is 600 $\mu$g/cm$^2$ with 230 $\mu$g/cm$^2$ of $^{10}$Be. The target is deposited on a 4.9 mg/cm$^2$ of platinum. In order to stop the beryllium and boron recoils a thick (40 mg/cm$^2$) Au backing was added. To suppress the reactions on the Au backing a beam energy of 29.4 MeV was chosen to be below the Coulomb barrier for the $^{7}$Li + $^{197}$Au system. To protect the silicon detectors against elastically scattered $^{7}$Li-particles aluminium-absorber foils, were used.

In this experiment, the reconstruction of the kinematics (see Section 2.3.3.) using the emitted $\alpha$ particles is not used because the recoiling nuclei stop in the target. Moreover the break-up reactions of $^{7}$Li on the backing resulted in a huge amount of chance light particle events in the ISIS detectors which leads to reduced statistics in the $\gamma$-$\gamma$-particle coincidences. One should keep in mind that the $^{10}$Be target was in the form of BeO and this results in a large amount

of reactions induced on $^{16}$O which complicated the data analysis.

A simple Doppler shift correction for the recoiling nuclei in the beam direction by varying $\beta$ and optimising the peak width for certain nuclei was made. The advantage of such a thick target experiment is that the full range of emitted recoils is accepted and that for $\gamma$-ray transitions emitted from excited states which have lifetimes longer than the stopping time ($\sim$1 ps), no Doppler shift correction is needed.

## 3.4 Results and discussion

The results presented below are from the experiment described in Section 3.3, using the $^{10}$BeO target and the $^{7}$Li beam. The reactions on $^{16}$O yielded new results about the band structure in the mirror nuclei $^{21}$Ne and $^{21}$Na (see Chapter 4), but contaminated the data for the beryllium isotopes. Despite this and the break up reactions on the backing of the $^{10}$Be target $\gamma$-ray transitions from the bandheads of the proposed molecular rotational bands in $^{10}$Be were observed.

### 3.4.1 $^{10}$Be

#### Intensities of $\gamma$-ray decays

Levels both under and above the particle emission threshold in $^{10}$Be were populated and the $\gamma$-decay scheme for the levels under the particle threshold was extracted (see Fig. 3.4). A representative spectrum gated by the 3367 keV transition from the $2_1^+$ to the ground state is shown in Fig. 3.5.

The $2^-$ level at an excitation energy of 6.26 MeV is several keV under the $^{9}$Be+$n$ threshold. Since the decays of all other levels under the threshold are observed except this one it is likely that the negative parity states are not populated in this reaction or that the $2^-$ level has a very short lifetime (less than femtoseconds) making the expected strong $E1$ (99% $\gamma$-ray branch) transition to

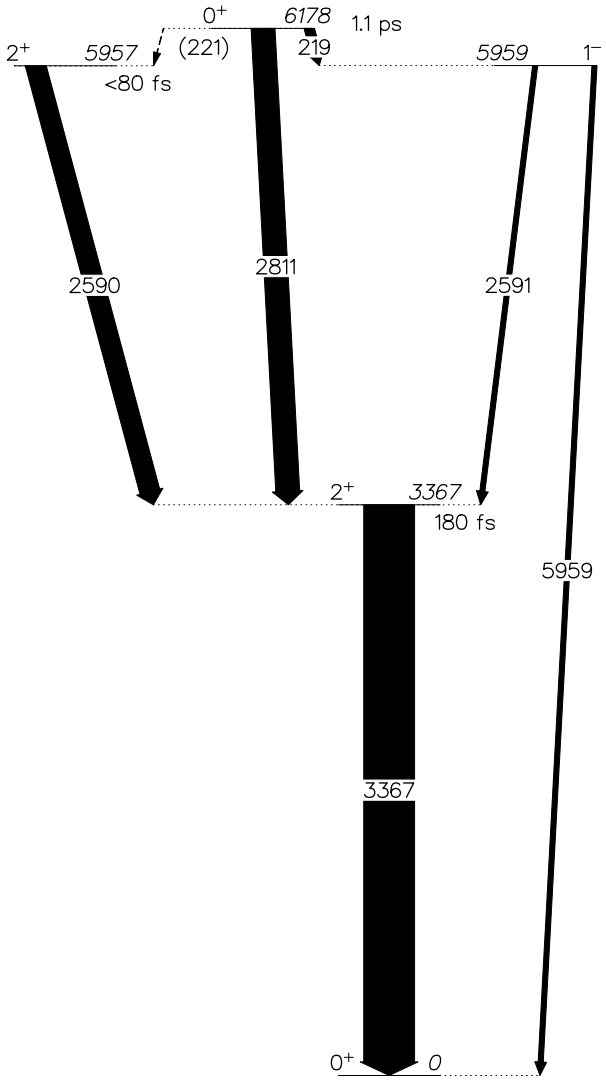


Figure 3.4: Decay-scheme for $^{10}$Be as observed in this experiment. The widths of the arrows correspond to the relative intensities of the $\gamma$-ray transitions. Energies are in keV.

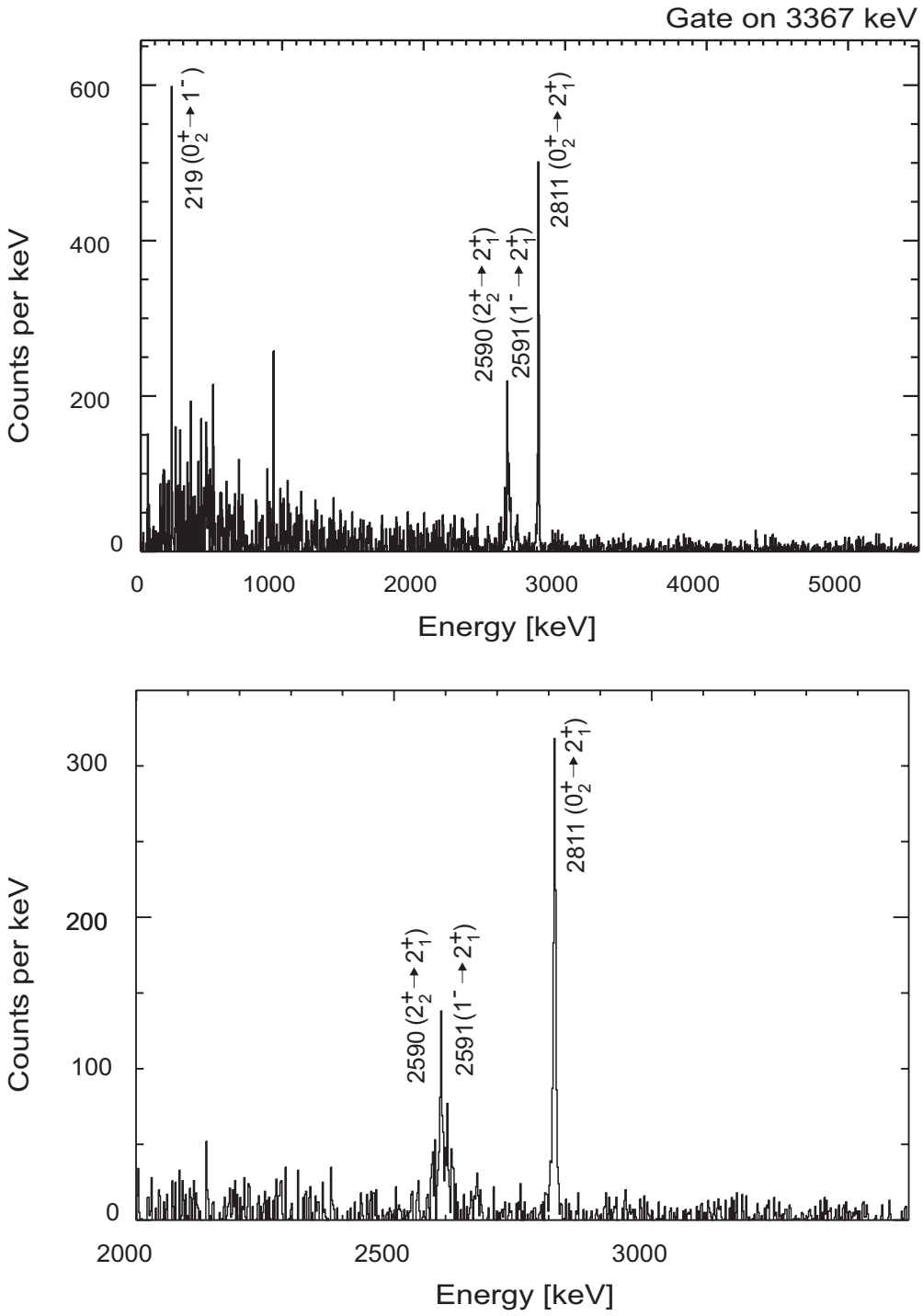


Figure 3.5: The top panel shows the $\gamma$-ray spectrum gated by the 3367 keV transition to the ground state in $^{10}$Be. The lines at the beginning of the spectrum ($\leq$1000 keV) are due to reactions on the backing of the target (Au and Pt) and $^{16}$O. The bottom panel shows the expanded part of the spectrum, clearly showing the 2590 keV doublet.

the $2_1^+$ state at an excitation energy of 3367 MeV very broad in the observed spectra. Since the other observed negative parity state ($1^-$) at 5.959 MeV forms a doublet with the $2_2^+$ state, it is impossible to say if the $1^-$ level is populated via $\gamma$-ray decay from other negative parity states or directly in the reaction. However, the $1^-$ state discussed here is populated from the isomeric $0_2^+$ state at 6.18 MeV. This leads to a sharp component in the observed $\gamma$-ray coincidence spectra, see, for example, Fig. 3.6.

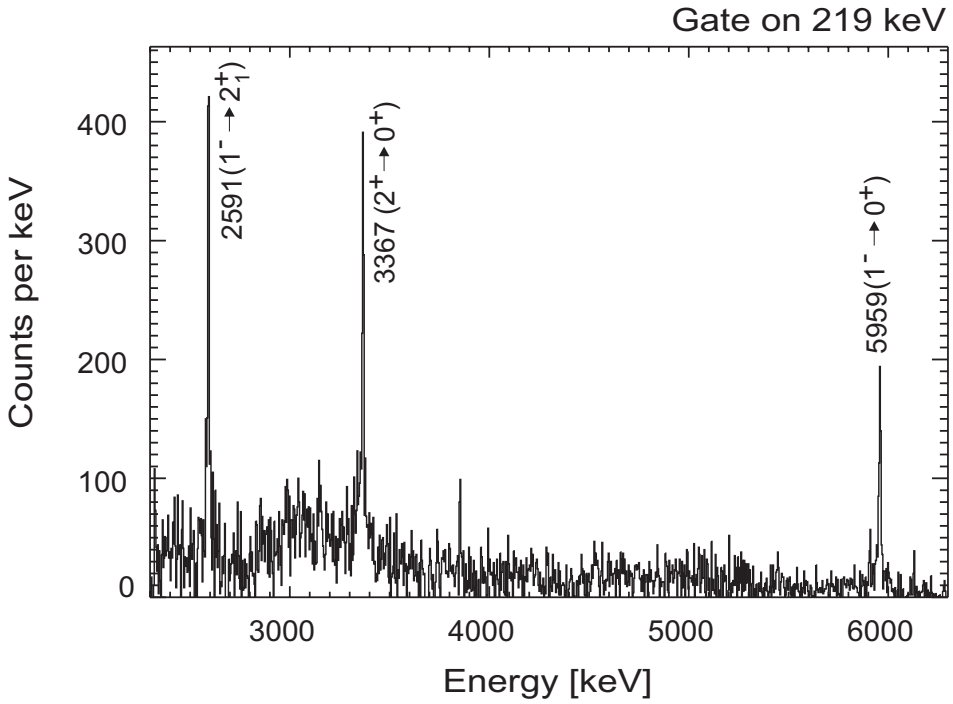


Figure 3.6: Gamma-ray spectrum gated by the 219 keV $E1$ transition from the isomeric $0_2^+$ state at an excitation energy of 6.18 MeV in $^{10}$Be. The sharp components of the subsequent transitions can be clearly seen.

To deduce the relative intensities of the $\gamma$-ray transitions in $^{10}$Be, an arbitrary, normalised intensity of 100 was taken for the 3367 keV $2_1^+ \rightarrow 0^+$ transition (see Table 3.4).

The intensities of the transitions were (when possible) directly deduced from the gate on the 3367 keV ground-state band transition, assuming I(2811) + I(2590

| | Transition energies [keV] | | | | |
|---|---|---|---|---|---|
| | 219 | 2591 | 2811 | 3367 | 5759 |
| Gate [keV] | Intensities [arb.] | | | | |
| 219[a] | | 40±3 | | 36±3 | 24±3 |
| 2591* | 25±3 | | | 75±2 | |
| 2811 | | | | 100 | |
| 3367 | 11±10 | 78±2 | 22±3 | | |
| 5759* | 100 | | | | |

Table 3.4: Relative intensities of the $^{10}$Be transitions as deduced from the $^{7}$Li+$^{10}$Be reaction, normalised to the 3367 keV, $2^+ \rightarrow 0^+$ transition. The doublet transitions are marked with '$*$' and the possible new 219 keV doublet transition with (a).

+ 2591) = 100 (see Fig. 3.4). From these data the branching ratio of the $1^-$ decay is different from the published value. Instead of a ratio of 83:17 [AS88], the 2591 and 5959 keV transitions are approximately equally strong. Unfortunately, it is difficult to give an exact ratio because of the large background, but the difference between these two transitions is not greater than 10 percent. The energy difference between the $1^-$ and the $2_2^+$ levels is 1.5±0.5 keV. This means that the newly observed 219 keV transition could be a doublet decaying to both the 5959 and 5957 keV levels. When gating on the 219 keV transition (see Fig. 3.6), the 2591 keV decay is more intense than expected from the literature [AS88].

In addition, the 3367 keV transition appears broadened when gating on the 2591 keV transitions (see Fig. 3.7). This suggests that the $2_2^+$ and/or $1_1^-$ levels are populated directly in the reaction or via prompt $\gamma$-ray decays from higher lying states. It is possible that this population is the origin of the difference in

the measured branching ratios.

Since the $0_2^+$ isomeric state at an excitation energy of 6178 keV is very weakly populated via neutron decay from $^{11}$Be (see Fig. 3.8), in the current data it is likely to be populated from higher lying levels, above the particle threshold. Such transitions have not been observed, perhaps because the initial levels are very broad giving rise to a large variation in the subsequent $\gamma$-ray decays.

The probability of populating the $2_2^+$ level through inelastic scattering can be negated since the 5957 keV transition from the $2_2^+$ level directly to the ground state is very weak. In addition, the possible population from the $0_2^+$ state is also very weak.

In the current work, it was proven that the $2_2^+$ bandhead (at 5957 keV) was populated by observing the linking $\gamma$-ray transitions to the ground-state band. This also confirmed the population of the proposed molecular bands in $^{10}$Be (see Fig. 3.3) since the states at 5957, 5959 and 6178 keV are all considered as band-heads of molecular structures. After $\beta$-decay of $^{11}$Li to $^{11}$Be the direct population of the $2_2^+$ and $1^-$ levels, via neutron decay has not been observed [Mor97]. The neutron decay of $^{11}$Be mainly populates the ground state and the first excited state in $^{10}$Be (see Fig. 3.8).

Below, various aspects relating to the cluster structure of particular states in $^{10}$Be will be discussed.

### The ground state ($0^+$) and the $2^+$ (3.37 MeV)

Both of these states are strongly populated in various one-nucleon transfer reactions on $^9$Be, suggesting that their structure is not very different. The strong E2 transition ($B(E2)$=10.5±1.2 $e^2fm^4$) between the $2^+$ and the $0^+$ states is an indication of their large deformation. Furthermore, new calculations from Kanada En'yo *et al.* [KE99] and Itagaki *et al.* [Ita00] show that both states are likely to have a cluster structure. The two $\alpha$-clusters here are closer together than in

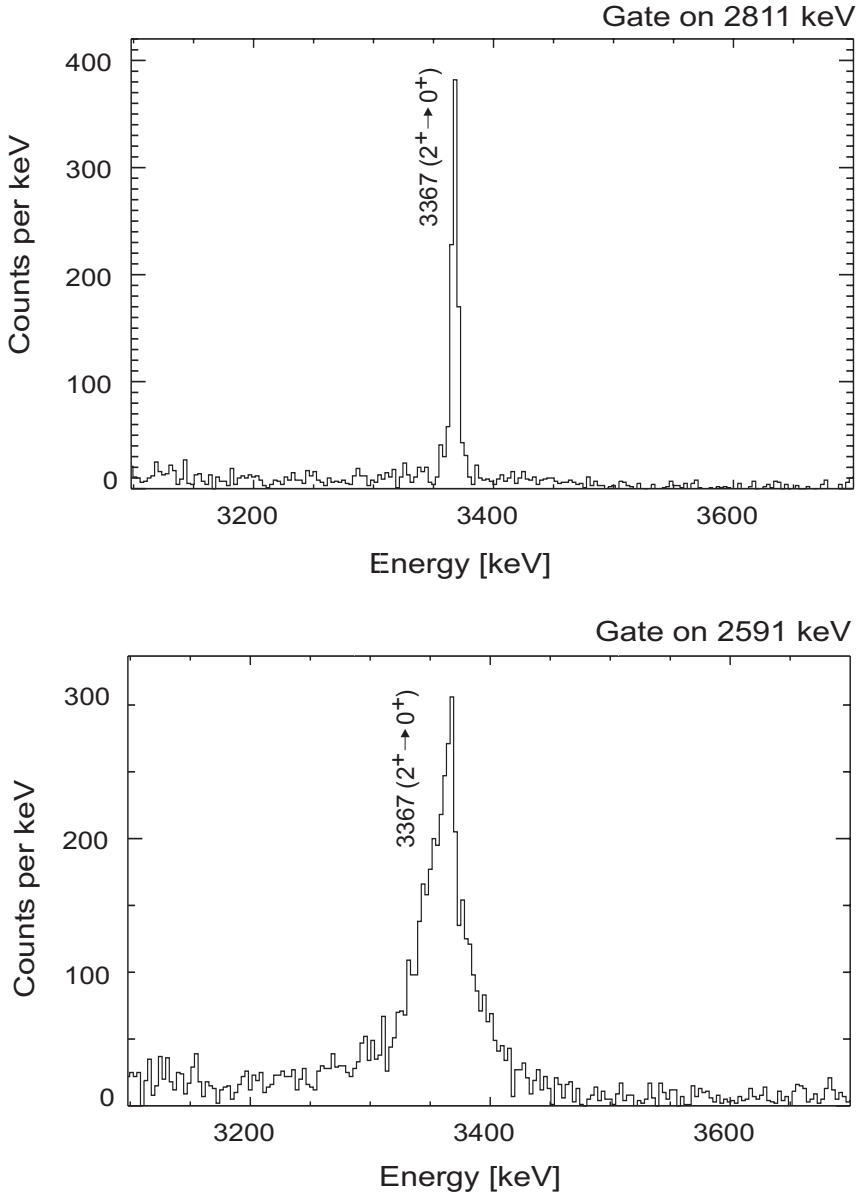


Figure 3.7: Top panel: $\gamma$-ray spectrum gated by the 2811 keV transition from the isomeric $0_2^+$ state. The sharp nature of the 3367 keV transition is clear. Bottom panel: $\gamma$-ray spectrum gated by the 2591 keV (doublet) transition in $^{10}$Be. The 3367 keV transition now appears broadened indicating a short (∼femtoseconds) lifetime component, perhaps as a result of direct population in the reaction or prompt $\gamma$-ray feeding.

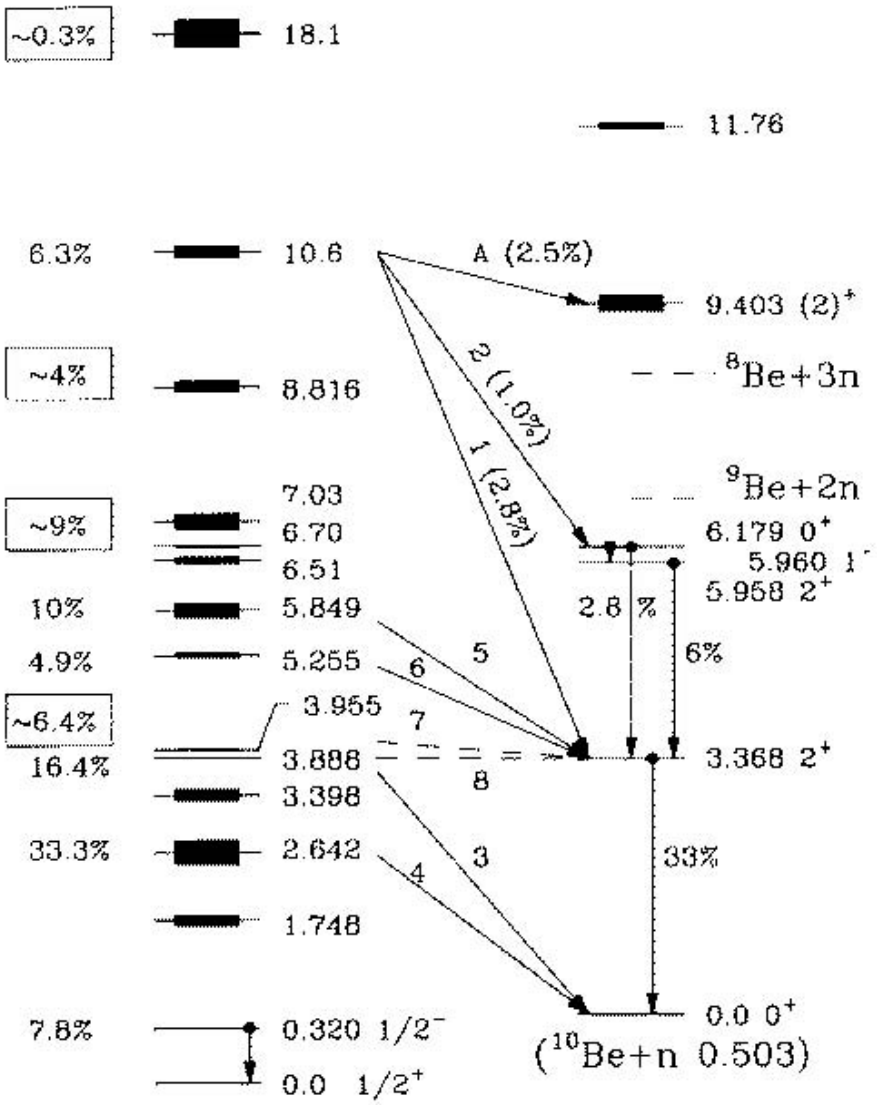


Figure 3.8: A schematic diagram of the neutron and $\gamma$-ray transitions taken from [Mor97]. On the left, the $\beta$-decay branching ratios from $^{11}$Li to energy levels in $^{11}$Be. On the far right are the energy levels in the neutron-decay daughter $^{10}$Be. The energies of the states are given in MeV and their widths are qualitatively indicated by the line thickness.

$^{8}$Be which is expected since the energy difference between these two levels, 3.37 MeV in $^{10}$Be, is bigger than the corresponding value in $^{8}$Be (3.04 MeV). In the current work a strong E2 transition (3367 keV) between these two states, the $2^+$ at 3367 keV and the ground state in $^{10}$Be, was observed, which is in good agreement with previous experimental results.

### $2_2^+$ ( 5.958 MeV), $1^-$ (5.959 MeV), $0_2^+$ (6.179 MeV) and $2^-$ (6.263 MeV)

These states are important since they prove the existence of a two-centre molecular structure in this A=10 nucleus [vO96b, vO97]. Earlier, the $0_2^+$ state in $^{10}$Be was an object of special interest, as it was considered as a candidate for an intruder level, having a configuration of two neutrons in the sd-shell. This was confirmed by the results from one-nucleon transfer reactions to which its contributions were either weak, or unobservable. In recent cluster and molecular approximations it was suggested that the 6.18 MeV state ought to be an extended object with a well developed $\alpha$-2n-$\alpha$ cluster structure [vO96a, vO97, KE99, Ita00, Oga00]. In Ref. [KE99] it was found that this state should also have a developed $\alpha$-2n-$\alpha$ structure, but according to Ref. [Oga00], a small (0.01) $\alpha$-$^{6}$He spectroscopic factor is obtained.

### $3^-$ (7.37 MeV) and $2^+$ (7.54 MeV)

These two states are considered to be the first and second excited members of two different rotational bands, based on the $1_1^-$ and $0_2^+$ configurations, respectively. Both were found as resonances in the total neutron capture cross-section of $^{9}$Be, there, the $3^-$ state has a strong population and a width of $\Gamma$=15.7 keV [AS88]. The $2^+$ state is weakly populated and has $\Gamma$=6.3 keV [Boc51, Fos61, Lan64]. In the current work $\gamma$-ray transitions de-populating these levels were not observed. The reason for this is likely to be that the calculated $\Gamma_\gamma/\Gamma_{tot}$ ratio (see Table 3.3) is not reachable with the experimental set up used here. Alternatively, it could be that the transitions coming from these states are very broadened.

### 3.4.2 $^{11}$Be

Internal $\gamma$-ray decays from $^{11}$Be were not observed. The neutron emission threshold in this nucleus is rather low (500 keV) and up to now there is only one known level which decays to the ground state emitting a 320 keV ($1/2^- \rightarrow 1/2^+$) $\gamma$-ray. As can be seen from Fig. 3.9, in the current data the peak corresponding to this transition was not visible in the total projection spectrum. Since there are no other known transitions in this nucleus it was not possible to continue the investigation.

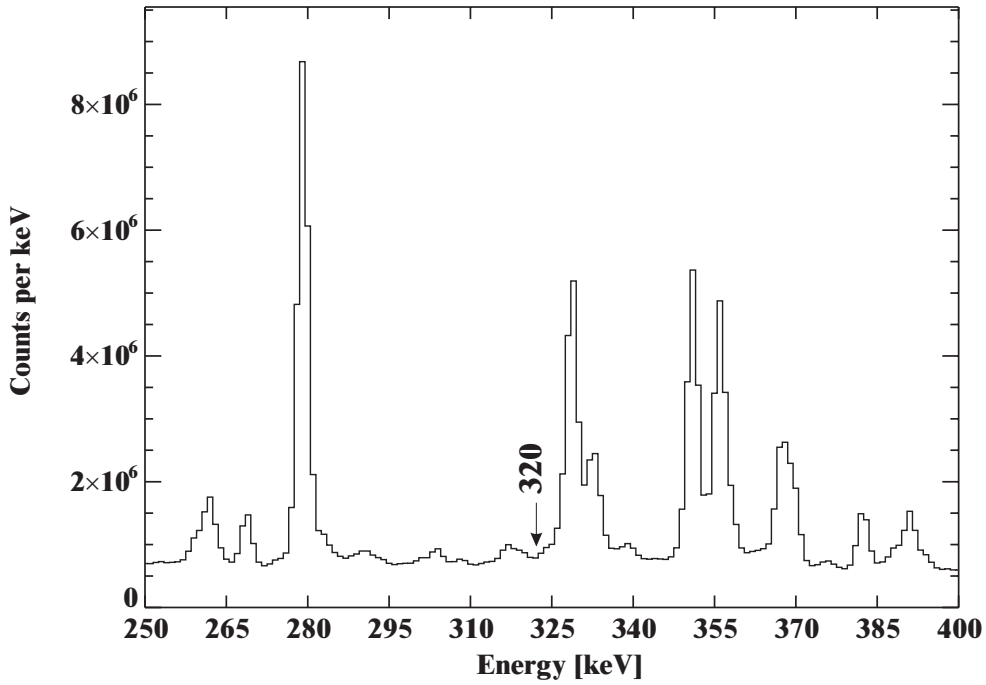


Figure 3.9: The part of the total $\gamma$-ray projection spectrum showing where the known transition at 320 keV to the ground state in $^{11}$Be should be.

### 3.4.3 $^{12}$Be

This nucleus has been studied recently [Shi03] and the experimental results show previously unobserved $\gamma$-ray transitions and prove the existence of an isomeric $0_2^+$ state at an excitation energy of 2.24 MeV, which decays to the first excited

$2^+$ state at 2.10 MeV following the emission of a 140 keV $\gamma$ ray. This 140 keV transition was observed in coincidence with the known 2.10 MeV ($2_1^+ \rightarrow 0_1^+$) transition. The isomeric state was produced by projectile fragmentation of $^{18}$O on a beryllium target [Shi03]. Looking again at other experimental data from Fortune *et al.* who measured the $^{10}$Be(t,p)$^{12}$Be reaction [For94], the population of the isomeric state is very weak. Consequently this state will not be populated (or only very weakly populated) in transfer reactions.

In the present data this energy region is difficult to reach because of contaminant background lines. Even if peaks are seen at the same energy (140 keV and 2100 keV) it is not possible to extract more information. One such contaminant is one of the $\gamma$-ray transitions to the ground state in $^{18}$F, which is at the same energy (2101 keV).

### 3.4.4 Gamma-ray coincidence data for the carbon isotopes

Gamma-ray transitions from known levels in $^{13}$C and $^{14}$C have also been observed (see Figs. 3.10 and 3.11). All transitions up to the particle thresholds in both nuclei were observed.

### 3.4.5 Summary and outlook

The $\gamma$-ray decay properties of neutron-rich isotopes of beryllium, close to the particle emission thresholds, have been studied. The results obtained are in agreement with the theoretical calculations. Some of the levels, even those expected to have large $\gamma$-ray transition probabilities are still beyond the reach of modern germanium detector arrays. For example, the 1.363 MeV transition in $^{10}$Be has a $B(E2)$ value of 35.72 $e^2fm^4$, but since this level is above the particle emission threshold the $\Gamma_\gamma/\Gamma_{tot}$ ratio is $2.1\times10^{-8}$ (see Table 3.3). Nevertheless, for the first time a complete $\gamma$-ray decay scheme for the levels up to the neutron

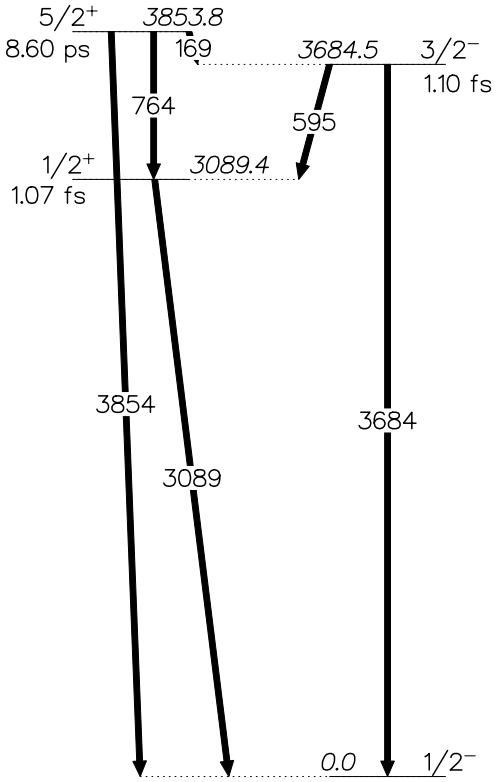


Figure 3.10: Decay-scheme for $^{13}$C as observed in this experiment. Energies are in keV.

decay threshold has been constructed. By comparing existing data to the current results, a new $\gamma$-ray transition from the isomeric $0_2^+$ state in $^{10}$Be was found. Furthermore, the population of the bandheads of the proposed rotational bands from levels above the particle thresholds was proven. Since these levels, the $2_2^+$ at 5958 keV and the $0_2^+$ at 6179 keV, are strongly populated and the $\gamma$-ray transitions above the particle thresholds feeding them are very weak, a direct population via neutron decay of $^{12}$Be and $^{11}$Be must be assumed from the 2n stripping reaction $^{10}$Be($^7$Li, $\alpha$p)$^{12}$Be$^*$.

The results of this experiment have been the basis for another experiment with a similar motivation, which was carried out recently and the data are still

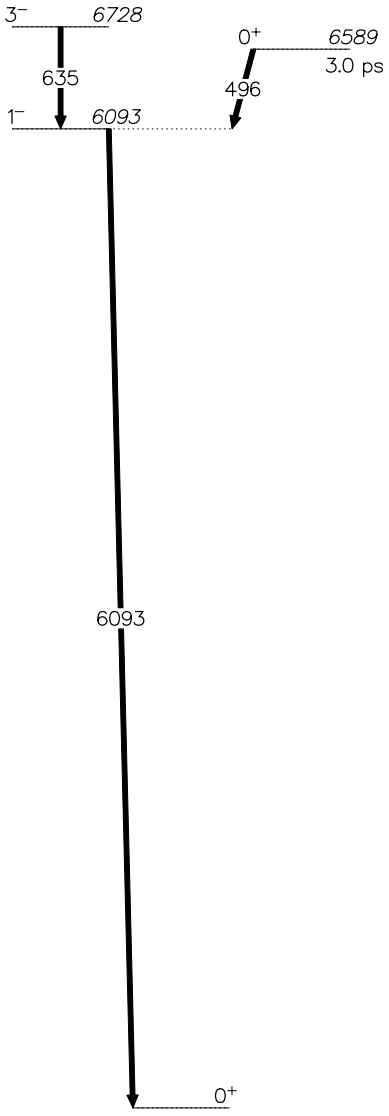


Figure 3.11: Decay-scheme for $^{14}$C as observed in this experiment. Energies are in keV.

under analysis. The new experimental set up includes the EUROBALL germanium array and the BRS (Berlin **B**inary **R**eaction **S**pectrometer) [Thu98] and is likely to detect some of the $\gamma$-ray transitions above the particle emission threshold described in Chapter 3.2. Such an experimental set-up enables $\gamma$-$\gamma$-particle and particle-particle-$\gamma$ coincidences to be measured. The selection of binary reactions enables a powerful pre-selection of the reaction channels to be made, implying that the EUROBALL array can be used mostly with one fold $\gamma$-ray multiplicities or with $\gamma$-$\gamma$-ray events, for which the total efficiency is 10 times higher than for GASP. The position information from the two BRS-detectors and the high granularity of Euroball can be used to achieve a high quality Doppler shift correction.